Article ID: 1000-324X(2019)05-0560-07 **DOI:** 10.15541/jim20180571

A Self-powered UV-visible Photodetector Based on p-Se/Al_2O_3/n-ZnO Nanorod Array Heterojunction

SUN Chao-Xiang, CHEN Liang, CHANG Yu, TIAN Wei, LI Liang

(Jiangsu Key Laboratory of Thin Films, School of Physical Science and Technology, Soochow University, Suzhou 215006, China)

Abstract: Self-powered photodetector is capable of transforming radiation signals to electronic signals without assistance of external power supply, which is widely utilized in industry and military. Herein, p-Se/n-ZnO nanorod array heterojunction was successfully synthesized and its application as UV-visible photodetector was explored. Due to the proper built-in electric field at the interface of ZnO and Se, the photogenerated electrons and holes are separated and transported in opposite directions, giving rise to high photocurrent at zero bias. Thus, this heterojunction can work as an independent and wireless self-powered photodetector. Introduction of Al_2O_3 interlayer between Se and ZnO efficiently reduces the dark current. The resulting device achieves high responsivity of 55 $\mu A \cdot W^{-1}$ and specific detectivity of 5×10^{10} Jones at 500 nm, as well as fast response speed (rise time of 0.9 ms and decay time of 0.3 ms).

Key words: ZnO; heterojunction; self-powered; photodetector

Photodetectors, which can convert radiation signals to electronic ones, have attracted enormous attention for a variety of industrial and military applications, including biological and chemical analysis, environmental monitoring, visible light communication, and space exploration[1-7]. Particularly, photodetectors working without consuming external power source, namely self-powered photodetectors, are urgently required to meet the demand of modern optoelectronic devices in the trend of lightweight and energy saving[8-9]. Self-powered photodetectors are usually constructed on hetero or Schottky junction. By exploiting the built-in electric field at the junction interface, photodetectors can detect the light signals at zero bias without consuming any external power[10].

Currently, utilization of low-dimensional wide-bandgap semiconductor nanomaterials, such as ZnO[11], SnO_2[12], ZnS[13-14], Nb_2O_5[15] and GaN[16], has attracted intense attention to develop high performance photodetectors. As a typical II-VI group compound semiconductor, zinc oxide (ZnO), possesses wide direct band gap (3.37 eV), large exciton binding energy (60 meV), high carrier mobility exceeding 100 $cm^2 \cdot V^{-1} \cdot s^{-1}$ at room temperature, and high resistance to irradiation[17]. These unique features make ZnO a promising candidate for photodetectors. Particularly, one-dimensional ZnO nanorods are usually utilized to construct photodetectors, due to their high crystallinity, large BET area and excellent carrier transport property. However, ZnO photodetectors usually suffer from low responsivity and specific detectivity due to a large number of trap states within ZnO, and slow response originating from the oxygen adsorption and desorption processes. Tremendous efforts have been made to improve the performance of ZnO based photodetectors, such as surface modification or construction of Schottky junctions.

As an intrinsic p-type semiconductor with small bandgap (1.6 eV), selenium (Se) is an ideal material to construct UV-visible broadband photodetector[18]. There are many unique physical and optical properties for Se. For instance, its melting point is as low as 217 ℃, and its conductivity is in the range of 10^{-6}–10^{-5} $\Omega^{-1} \cdot cm^{-1}$. In addition, Se possesses a high hole mobility up to 0.63 $cm^{-1} \cdot V^{-1} \cdot s^{-1}$ and large hole carrier concentration of 9.35×10^{16} cm^{-1}[19-22]. Novel piezoelectric, thermoelectric and non-linear optical response were observed in Se. Recently, Se based photodetectors with various structures, such as thin film, nanowire, nanobelt and so on[19,23-24], were fabricated and demonstrated respectful performance in photodetection. To improve the performance, Se was integrated with TiO_2 and organic semiconductor to form heterojunction[25-26]. For example, Yu, *et al*[26] fabricated a self-powered UV-visible photodetector based on com-

Received date: 2018-12-04; **Modified date:** 2018-12-26
Foundation item: National Natural Science Foundation of China (51502184, 51872191); College Students' Innovation and Entrepreneurship Training Program (201710285084X)
Biography: SUN Chao-Xiang(1995–), male, undergraduate. E-mail: 2196728627@qq.com
Corresponding author: TIAN Wei, associate professor. E-mail: wtian@suda.edu.cn; LI Liang, professor. E-mail: lli@suda.edu.cn

posite structure of single Se microtube and conducting polymers. The optimum device exhibited high on/off ratio of 1.1×10^3, large detectivity (3.78×10^{11} Jones) and high response speed (rise time of 4.5 μs and fall time of 2.84 ms) at zero bias voltage and 610 nm. Hu, *et al*[27] fabricated a photodetector by depositing plasmonic metallic nanoparticles on the Se microtube by utilizing both the heterojunction and surface plasmon coupling effect. The device demonstrates broadband photoresponse from 300 to 700 nm with peak responsivity of about 19 $mA\cdot W^{-1}$ at 610 nm and response time of 0.32 ms. Despite these achievements, many associated problems, including interface defects caused by lattice mismatch between hetero-materials, low mobility of organic semiconductor and complex fabrication process, not only bring about obstacles to the fabrication of composite structures but also degrade the photodetecting performances.

In this work, we report the fabrication of p-Se/n-ZnO nanorod array heterojunction, and its integration into a self-powered and rapid-response UV-visible photodetector. The resulting device exhibits fast response with a rise time of 0.9 ms and decay time of 0.3 ms. Meanwhile, the device achieves the peak responsivity and specific detectivity of about 55 $\mu A\cdot W^{-1}$ and 5×10^{10} Jones at 500 nm, respectively.

1 Experimental

The fabrication process of p-Se film/n-ZnO nanorod array heterojunction is illustrated in Fig. 1. Firstly, the fluorine doped tin oxide (FTO) glass was cut into 1 cm × 1.5 cm small pieces, cleaned with acetone, ethanol and deionized water in sequence for 10 min each step, and dried with nitrogen. Then the prepared FTO was subject to UV radiation for 20 min to improve its hydrophilic property. Afterward, 40 nm ZnO seed layer was deposited on FTO by atomic layer deposition (ALD) and then annealed at 500 ℃ for 60 min. For the growth of ZnO nanorods, zinc nitrate hexahydrate ($Zn(NO_3)_2$) (25 mmol/L) and hexamethylene tetramine (HMTA) (25 mmol/L) were dissolved in deionized water, and followed by stirring for 2 h. After that, the substrates were immersed into the solution with the conductive side facing down. Then the beaker was heated to 90 ℃ and maintained for 6 h in a thermostatic water bath. After the reaction completed, the sample was cleaned by deionized water several times, and then dried in a vacuum oven. To get crystallized ZnO nanorods, the sample was annealed at 500 ℃ for 60 min in a muffle furnace. Then, 2 nm Al_2O_3 film was deposited on the ZnO nanorod array by ALD. For the growth of Se film, a vapor transport and deposition process were

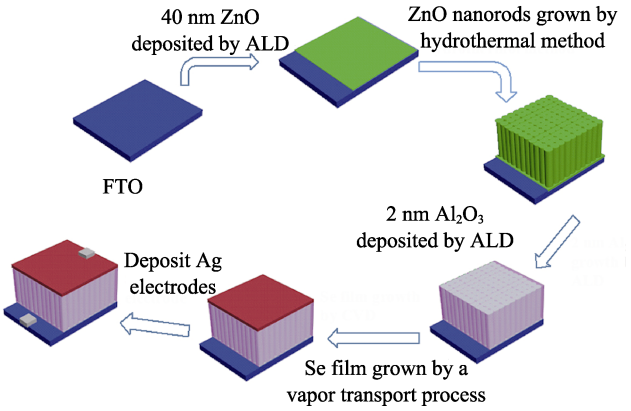

Fig. 1 Schematic illustration of the fabrication process of the p-Se film/n-ZnO heterojunction

performed in a horizontal tube furnace. A ceramic boat containing 3 g Se powder was placed in the middle of the quartz tube. ZnO and Al_2O_3 coated FTO substrate was put 30 cm away from the Se source. To eliminate air in the furnace, pure nitrogen was aerated for 2 h with the speed of 300 sccm. Then the speed was changed to 200 sccm for deposition. During the deposition, the furnace was heated to 380 ℃ and maintained for 4 h. Finally, 100 nm Ag was thermal-evaporated on the surface of Se film as top electrode. The active area of device is 15 mm^2.

The morphology of the ZnO nanorod array and Se film was characterized using a field emission scanning electron microscope (FE-SEM, Hitachi, SU8010). The crystalline and structural properties of the layers were investigated by X-ray diffraction (XRD, D/MAX–III–B-40 KV, Cu Kα radiation, λ=0.15418 nm). The absorption spectra of the ZnO and ZnO/Se were measured using a UV-visible spectrometer (Shimadzu, UV-3600). The photoelectric properties of the obtained photodetectors, including current-voltage (*I-V*) curves, spectra responsivity, and time-dependent photoresponse (*I-t*), were characterized using a semiconductor characterization system (Keithley 4200) under 100 $mW\cdot cm^{-2}$ simulated solar light (Newport, 94043A) and monochromatic light produced with monochromator (Zolix, Omni-λ 3009) using order sorting filters. The light intensity was measured by a power meter (Newport, 1936-R). The response speed was recorded by an oscilloscope (Tektronix, MSO 58). The lasers (FU405 AL200-GD16 and FU650AD5-GC12) were used as light sources during measurement of the relationship between photocurrent and light intensity. The power intensity of laser can be tuned by changing the DC current.

2 Results and discussion

Fig. 2 shows the top-view and cross-sectional SEM

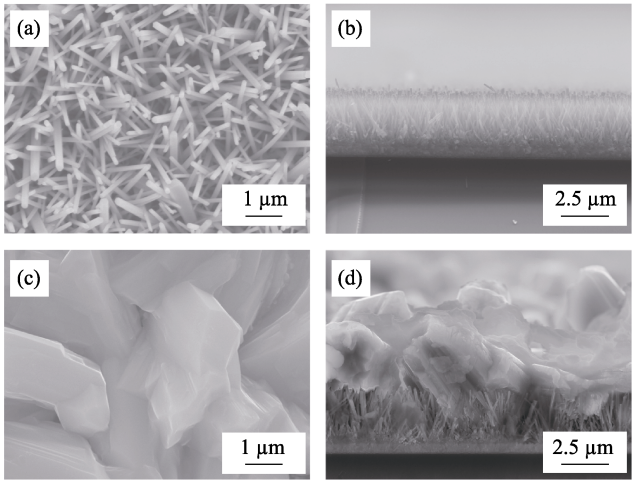

Fig. 2 SEM images of (a–b) ZnO and (c–d) p-Se/n-ZnO heterojunction
(a, c) Top view; (b, d) Cross-sectional view

images of the p-Se/n-ZnO nanorod array. As shown in Fig. 2(a), the ZnO nanorod array vertically align on FTO substrate with diameter of 50–150 nm. The length of ZnO nanorod array is about 2.5 μm (Fig. 2(b)). Fig. 2(c) reveals that Se film is composed of large crystals. The cross-sectional image in Fig. 2(d) reveals that the deposited Se film is around 3 μm thick and an intimate contact is formed at the interface between Se film and ZnO nanorod.

XRD pattern of the p-Se/n-ZnO nanorod array is plotted in Fig. 3(a). All peaks attained are in well agreement with the characteristic peaks of wurtzite ZnO (JCPDS 36-1451) and Se (JCPDS 06-0362). The sharp and strong peaks demonstrate that both ZnO and Se own high crystallinity. The relative intensity of ZnO (002) peak is much stronger than those of other peaks, indicating ZnO nanorods possess a preferred orientation with *c*-axis perpendicular to the substrate. The comparative UV-visible absorption spectra of pure ZnO and Se/ZnO are shown in Fig. 3(b). The pure ZnO nanorod array exhibits absorption when the light wavelength is below 368 nm, which corresponds to the bandgap of ZnO (3.37 eV)[28-29]. Upon deposition of Se film, there is an apparent absorption enhancement in visible light region. And the absorption edge is red-shifted to 730 nm, which is in consistence with the bandgap of Se (1.7 eV)[30].

Fig. 4(a) and (b) represent the typical *I-V* characteristics of the device under dark, white light and monochromatic light. The significantly enhanced current under light illumination at zero bias voltage can be obviously detected. And the photocurrent curve does not pass the zero point, which means the device can work in self-powered mode. In comparison, *I-V* curve of the device without Al_2O_3 interlayer shows a great dark current under white light illumination in the inset of Fig. 4(a). Fig. 4(c) and (d) represent the *I-t* curves of the device under periodic light on-off cycles at zero bias voltage. As shown in Fig. 4(c), the current obviously shows two distinct states when the white light irradiation is on and off, respectively. The dark current is only 2.2 pA; nevertheless, the photocurrent is remarkably boosted to a stable value of 435 pA, delivering a high on-off ratio (photocurrent to dark current ratio) of about 200. Fig. 4(d) shows the photoresponse of the device under 405 nm (1.664 μW·cm^{-2}), 532 nm (1.543 μW·cm^{-2}) and 650 nm (1.093 μW·cm^{-2}) monochromatic light illumination. Reproducible and stable photoresponse is observed for the device. Environmental stability is a key parameter of photodetector, which is crucial to its practical application. *I-t* curve of the device under 500 nm illumination for 10 min is shown in Fig. 4(e). Noted that the device is exposed to air in ambient conditions without any encapsulation.

There is no obvious degradation for photocurrent after 10 min measurement, indicating its superior stability. Responsivity and detectivity are two important parameters to characterize the capability of a photodetector. Fig. 4(f) shows the spectral responsivity and detectivity from 300 to 800 nm for the device at zero bias voltage. It is revealed that the device exhibits obvious response to UV-visible light with a decrease at about 730 nm, which corresponds to the band gap of Se. Defects existed in Se film can introduce energy levels in the forbidden band,

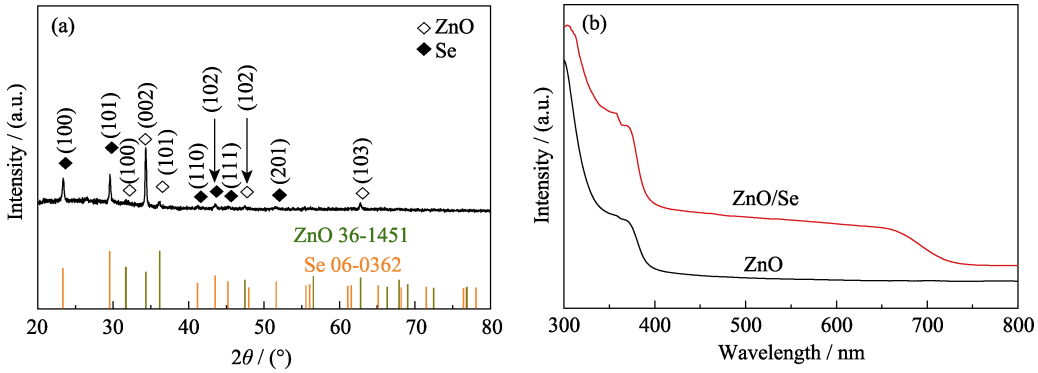

Fig. 3 (a) XRD pattern of p-Se film and n-ZnO nanorod array, and (b) absorption spectra of pure ZnO and Se/ZnO hybrid structure

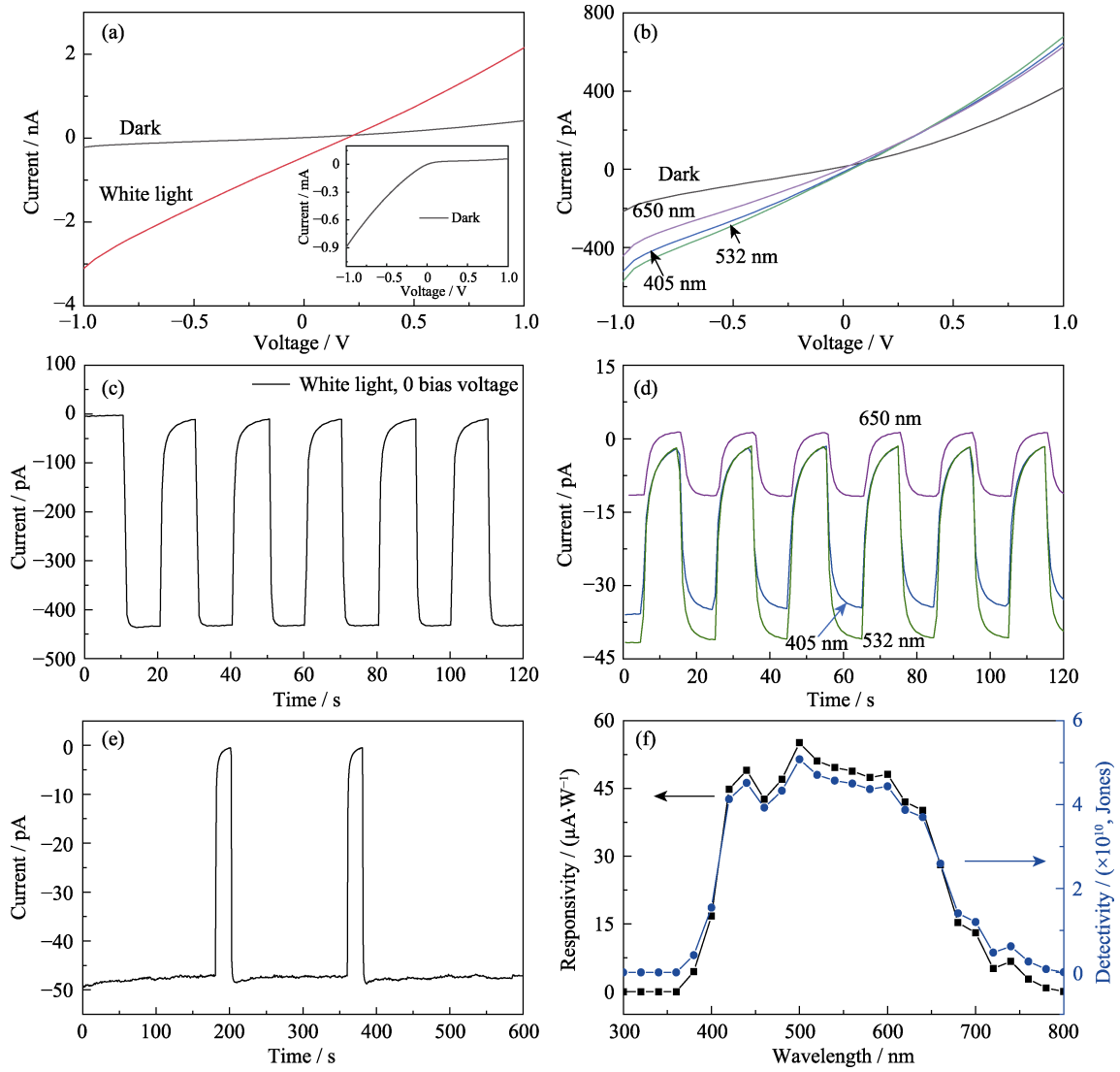

Fig. 4 Typical *I-V* curves for Se-Al_2O_3-ZnO device under (a) dark, white light and (b) dark, monochromatic lights; *I-t* curves of the device under (c) dark, white light and (d) dark, monochromatic lights; (e) Long-term response of the device under 500 nm illumination; (f) Spectral responsivity and detectivity of the device at 0 bias voltage

which allows Se to absorb photon with energy less than its bandgap. Thus, there is still response between 730–800 nm. The heterojunction device has the peak responsivity and specific detectivity of 55 $\mu A \cdot W^{-1}$ and 5×10^{10} Jones at 500 nm illumination, respectively. In comparison to the high responsivity in visible light region, the responsivity in UV region is relatively low. The responsivity at 320, 340 and 360 nm is 1.54, 1.15 and 1.57 $nA \cdot W^{-1}$, respectively. The low responsivity in UV region is possibly because the light illuminates on the device from ZnO side. Due to the wide bandgap of ZnO, UV light is mainly absorbed by ZnO, generating electron-hole pairs. However, the holes cannot transit to the top electrode (Ag) to be collected because of the thick Se film, thus giving rise to low photocurrent and responsivity in UV region.

Fig. 5(a) and (c) show the *I-t* curves of the Se/Al_2O_3/ZnO heterojunction device under illumination of 405 and 650 nm lasers with varying intensities. The photocurrent increases gradually with the light power intensity increasing. The corresponding photocurrents as functions of light intensities are shown in Fig. 5(b) and (d). The photocurrents strongly depend on the light power densities, and the dependence can be described by the power law[10]:

$$I_p \sim P^{\theta} \quad (1)$$

where I_p represents the photocurrent, P is the power density of the incident light, and θ is an exponent[9]. The fitting curves show that θ=0.57 and 0.50 for the wavelength of 405 and 650 nm, respectively. The non-unity exponents suggest a complex process of electron-hole generation, recombination, and trapping within the Se/ZnO nanorod array.

A designed circuit diagram for characterizing the response speed is shown in Fig. 6(a). Fig. 6(b) presents the response speed testing, where the device was illuminated

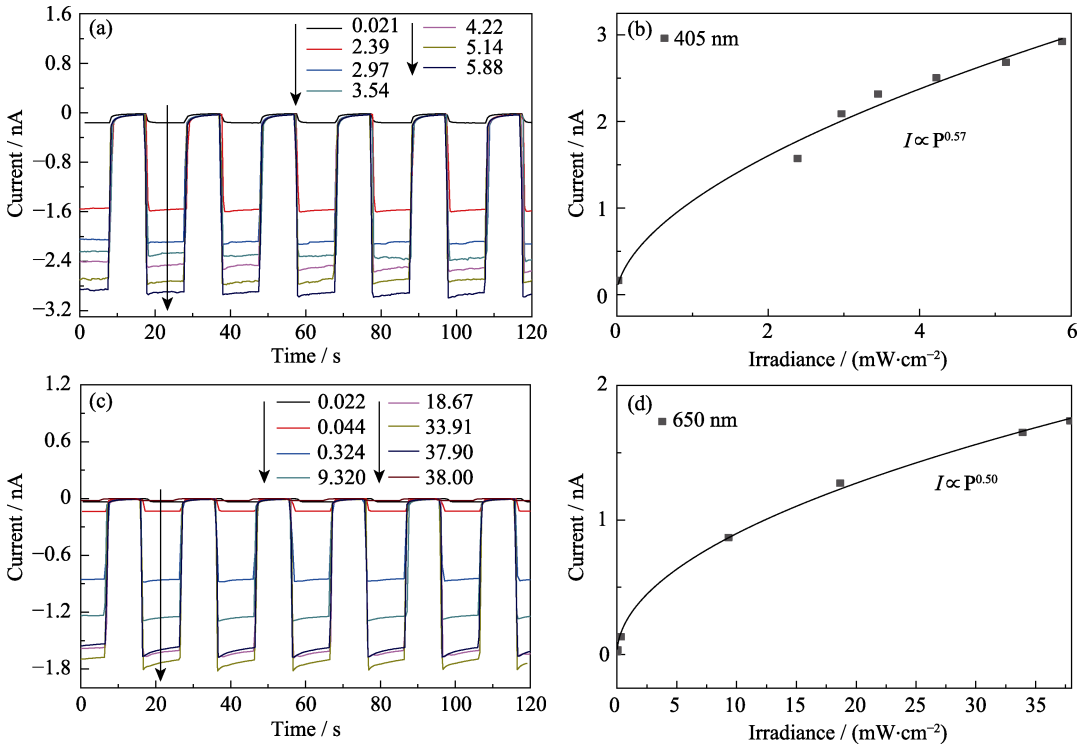

Fig. 5 *I-t* curves of the Se/Al_2O_3/ZnO heterojunction device under illumination of (a) 405 nm and (c) 650 nm lasers with varying light intensities (The unit of the light power is mW·cm^{-2}); Relationships between the photocurrent and the light intensity at 0 bias voltage under illumination of (b) 405 and (d) 650 nm lasers

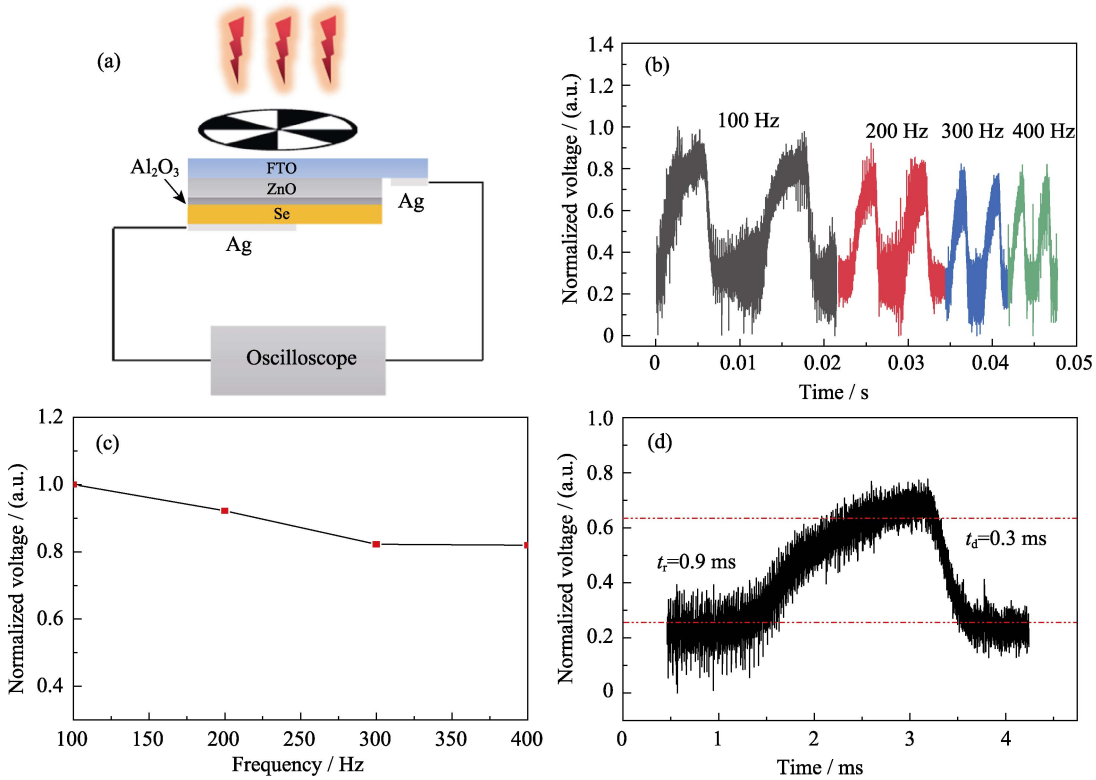

Fig. 6 (a) Diagram of electric circuit to characterize the response speed; (b) Time-dependent voltage curves at different chopper frequency; (c) Normalized voltage-frequency curve; (d) Enlarged one response cycle with rise and decay time

with the chopped laser of 100, 200, 300, 400 Hz. A decreased response is shown with increasing frequency of the chopped laser in Fig. 6(c). To characterize the real response speed, one response cycle is enlarged. The rise time (t_r) and decay time (t_d) are defined as the values needed for the dark current to reach 90% of the maximum

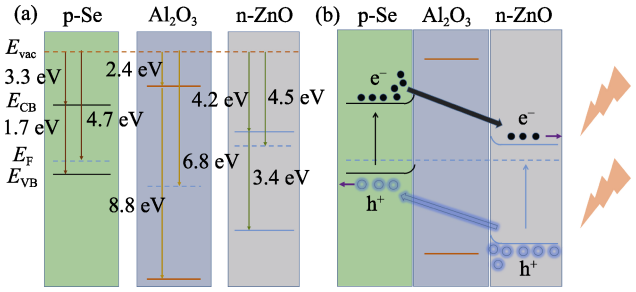

Fig. 7 Energy-band diagrams of the p-Se/Al_2O_3/n-ZnO nanorod array device (a) before and (b) after contact

photocurrent and down to 10% *vice versa*, respectively. It is found that t_r and t_d of the device are 0.9 and 0.3 ms, respectively, as shown in Fig. 6(d).

To disclose the work mechanism of the photodetector, an energy band diagram of the Se-Al_2O_3-ZnO is plotted in Figure 7. Before contact, Fermi level of ZnO is higher than that of Se (Fig. 7(a)). Once contact takes place, electrons would drift from ZnO to Se until Fermi levels line up. Upon illumination, well-aligned energy-band structure could separate the photogenerated electron-hole pairs in ZnO and Se at the heterojunction interface and help the charge carriers transport to electrodes, giving rise to large photocurrent.

As shown in Fig. 7(b), due to its particular band structure, Al_2O_3 interlayer prevents electron-hole recombination, which could efficiently decrease the dark current. Thus, the introduction of Al_2O_3 interlayer contributes to higher photo-dark current ratio, responsivity and detectivity.

3 Conclusions

In summary, a self-powered p-Se/Al_2O_3/n-ZnO UV-visible detector was prepared in this study. The self-powered functionality of the device is attributed to the proper built-in electric field between ZnO and Se arising from the well-aligned energy-band structure at the interface, which enables the photogenerated electrons and hole to separate and transport in opposite directions. Superior optoelectronic performances, including high responsivity (55 $\mu A \cdot W^{-1}$) and detectivity (5×10^{10} Jones), fast response speed (rise/decay time of 0.9/0.3 ms) are achieved for this device, which promise its potential application in light communication and image sensors.

References:

[1] ZHENG L, TENG F, ZHANG Z, *et al.* Large scale, highly efficient and self-powered UV photodetectors enabled by all-solid-state n-TiO_2 nanowell/p-NiO mesoporous nanosheet heterojunctions. *J. Mater. Chem. C*, 2016, **4(42):** 10032–10039.

[2] LIU X, GU L L, ZHANG Q P, *et al*. All-printable band-edge modulated ZnO nanowire photodetectors with ultra-high detectivity. *Nat. Commun*., 2014, **5:** 4007–4016.

[3] TSAI D S, LIU K K, LIEN D H, *et al*. Few-layer MoS_2 with high broadband photogain and fast optical switching for use in harsh environments. *ACS Nano*, 2013, **7(5):** 3905–3911.

[4] LU H, TIAN W, CAO F R, *et al*. A self-powered and stable all-perovskite photodetector–solar cell nanosystem. *Adv. Funct. Mater.*, 2016, **26(8):** 1296–1302.

[5] HATCH S M, BRISCOE J, DUNN S A. Self-powered ZnO-nanorod/CuSCN UV photodetector exhibiting rapid response. *Adv. Mater.*, 2013, **25(6):** 867–871.

[6] YANG Z, WANG M Q, DING J J, *et al*. Semi-transparent ZnO-CuI/CuSCN photodiode detector with narrow-band UV photoresponse. *ACS Appl. Mater. Interfaces*, 2015, **7(38):** 21235–21244.

[7] LI M, LIN C Y, YANG S H, *et al.* High mobilities in layered InSe transistors with indium-encapsulation-induced surface charge doping. *Adv. Mater.*, 2018, **30(44):** 1803690–1–10.

[8] BIE Y Q, LIAO Z M, ZHANG H Z, *et al*. Self-powered, ultrafast, visible-blind UV detection and optical logical operation based on ZnO/GaN nanoscale p-n junctions. *Adv. Mater*., 2011, **23(5):** 649–653.

[9] CHEN H Y, LIU K W, HU L F, *et al*. New concept ultraviolet photodetector. *Mater. Today*, 2015, **18(9):** 493–502.

[10] ZHANG H B, ZHANG X J, LIU C, *et al*. High-responsivity, high-detectivity, ultrafast topological insulator Bi_2Se_3/silicon heterostructure broadband photodetectors. *ACS Nano*, 2016, **10(5):** 5113–5122.

[11] SHEN Y W, YAN X Q, BAI Z M, *et al*. A self-powered ultraviolet photodetector based on solution-processed p-NiO/n-ZnO nanorod array heterojunction. *RSC Adv*., 2015, **5(8):** 5976–5981.

[12] FANG X S, YAN J, HU L, *et al*. Thin SnO_2 nanowires with uniform diameter as excellent field emitters: a stability of more than 2400 minutes. *Adv. Funct. Mater*., 2012, **22(8):** 1613–1622.

[13] FANG X S, BANDO Y, LIAO M, *et al*. Single-crystalline ZnS nanobelts as ultraviolet-light sensors. *Adv. Mater*., 2009, **21(20):** 2034–2039.

[14] LIU H, HU L, WATANABE K, *et al*. Cathodoluminescence modulation of ZnS nanostructures by morphology, doping, and temperature. *Adv. Funct. Mater*., 2013, **23(29):** 3701–3709.

[15] LIU H, GAO N, LIAO M, *et al*. Hexagonal-like Nb_2O_5 nanoplates-based photodetectors and photocatalyst with high performances. *Sci. Rep*., 2015, **5:** 7716–7725.

[16] LI D, SUN X, SONG H, *et al*. Realization of a high-performance GaN UV detector by nanoplasmonic enhancement. *Adv. Mater.*, 2012, **24(6):** 845–849.

[17] BAI Z, CHEN X, YAN X, *et al*. Self-powered ultraviolet photodetectors based on selectively grown ZnO nanowire arrays with thermal tuning performance. *Phys. Chem. Chem. Phys*., 2014, **16(20):** 9525–9529.

[18] QIN J, QIU G, JIAN J, *et al.* Controlled growth of a large-size 2D selenium nanosheet and its electronic and optoelectronic applications. *ACS Nano*, 2017, **11(10):** 10222–10229.

[19] LUO L B, YANG X B, LIANG F X, *et al.* Transparent and flexible selenium nanobelt-based visible light photodetector. *CrystEngComm*, 2012, **14(6):** 1942–1947.

[20] LIU P, MA Y, CAI W, *et al.* Photoconductivity of single-crystalline selenium nanotubes. *Nanotechnology*, 2007, **18(20):** 205704–1–5.

[21] MASUZAWA T, SAITO I, YAMADA T, *et al*. Development of an amorphous selenium-based photodetector driven by a diamond cold cathode. *Sensors*, 2013, **13(10):** 13744–13778.

[22] CHAMPNESS C H, SHUKRI Z A, CHAN C H. Minority carrier diffusion length determination from capacitance measurements in

Se-CdO photovoltaic cells. *Can. J. Phys*., 1991, **69(34):** 538–542.

[23] CHANG C Y, PAN F M, LIN J S, *et al.* Lateral amorphous selenium metal-insulator-semiconductor-insulator-metal photodetectors using ultrathin dielectric blocking layers for dark current suppression. *J. Appl. Phys.*, 2016, **120(23):** 234501–1–8.

[24] CHEN Y Z, YOU Y T, CHEN P J, *et al.* Environmentally and mechanically stable selenium 1D/2D hybrid structures for broad-range photoresponse from ultraviolet to infrared wavelengths. *ACS Appl. Mater. Interfaces*, 2018, **10(41):** 35477–35486.

[25] ZHENG L, HU K, TENG F, *et al.* Novel UV–visible photodetector in photovoltaic mode with fast response and ultrahigh photosensitivity employing Se/TiO_2 nanotubes heterojunction. *Small*, 2017, **13(5):** 1602448–1-11.

[26] YU P, HU K, CHEN H, *et al.* Novel p–p heterojunctions self-powered broadband photodetectors with ultrafast speed and high responsivity. *Adv. Funct. Mater.*, 2017, **27(38):** 1703166–1–10.

[27] HU K, CHEN H, JIANG M, *et al.* Broadband photoresponse enhancement of a high performance *t*-Se microtube photodetector by plasmonic metallic nanoparticles. *Adv. Funct. Mater.*, 2016, **26(36):** 6641–6648.

[28] SHAO D, YU M, LIAN J, *et al*. Heterojunction photodiode fabricated from multiwalled carbon nanotube/ZnO nanowire/p-silicon composite structure. *Appl. Phys. Lett*., 2013, **102(2):** 021107–1–3.

[29] TIAN C, JIANG D, LI B, *et al*. Performance enhancement of ZnO UV photodetectors by surface plasmons. *ACS Appl. Mater. Interfaces*, 2014, **6(3):** 2162–2166.

[30] YANG W, HU K, TENG F, *et al*. High-performance silicon-compatible large-area UV-to-visible broadband photodetector based on integrated lattice-matched type II Se/n-Si heterojunctions. *Nano Lett.*, 2018, **18(8):** 4697−4703.

基于 p-Se/Al_2O_3/n-ZnO 纳米棒阵列异质结的自驱动紫外–可见光探测器

孙超祥, 陈 亮, 常 宇, 田 维, 李 亮

(苏州大学 物理科学与技术学院, 江苏省薄膜重点实验室, 苏州 215006)

摘 要: 自驱动光探测器能够在无外加偏压的情况下将光信号转化为电信号, 在工业和军事领域有着广泛的应用。本研究报道了 p 型 Se 薄膜和 n 型 ZnO 纳米棒阵列异质结的可控合成以及它们作为自驱动紫外−可见光探测器的应用。由于在 ZnO 和 Se 的界面处形成的内建电场将光生电子–空穴对分离, 促使它们向相反方向传输, 最终被电极收集, 在 0 偏压下获得了较高的光电流(435 pA), 从而实现无线的自驱动光电探测。并且, 在 Se 和 ZnO 界面处沉积的 Al_2O_3 层有效降低了暗电流。最终, 此器件在 500 nm 的单色光下显示了高响应率 55 μA·W^{-1} 和大比探测率 5×10^{10} Jones, 并表现出了极快的响应速度(上升时间 0.9 ms, 衰减时间 0.3 ms)。

关 键 词: 氧化锌; 异质结; 自驱动; 光探测器

中图分类号: O472 **文献标识码:** A